Fatigue Response of Open Hole Plates: A Finite Element Simulation Investigating the Influence of Dynamic and Static Cold Expansion Processes

Guo Zheng [a, b], Zengqiang Cao [a, c], Yuehaoxuan Wang [a], Reza Talemi [b, *]

[a]Department of Mechanical Engineering, Northwestern Polytechnical University, Xi'an 710072, China

[b]Department of Materials Engineering, KU Leuven, 3001, Leuven, Belgium

[c]NPU Xu Hang Electromagnetic Technology Limited Company, Xi'an 710072, China

*Corresponding authors: reza.talemi@kuleuven.be

Abstract

Cold Expansion (CE) techniques are extensively used in the aeronautical industry to enhance the fatigue life of open-hole plates. However, the availability of accurate Finite Element (FE) models to simulate the fatigue behavior of this process, particularly Dynamic Cold Expansion (DCE), is limited. This study introduces two novel methods for predicting the fatigue response of DCE and Static Cold Expansion (SCE) open-hole plates. The first method directly estimates the total fatigue life using Continuum Damage Mechanics (CDM) and the Theory of Critical Distance (TCD). The second method separates the prediction of fatigue crack initiation life and propagation life, incorporating CDM, TCD, and the Extended Finite Element Method (XFEM). Moreover, FE models are developed to simulate residual stress, stress under external cyclic loads, and fatigue crack propagation behavior for both DCE and SCE specimens. The proposed methods are evaluated, compared, and the mechanisms behind fatigue life enhancement and fatigue crack propagation modes in CE specimens are discussed. It is found that the prediction accuracy is enhanced by considering stress distributions along the thickness direction and improving the Line Method (LM) in TCD through the introduction of a novel CE parameter. The results demonstrate that both methods achieve good predictive performance, with an average error index within ±30%. Furthermore, it is observed that both DCE and SCE processes primarily improve the fatigue crack initiation life of open-hole plates, with the percentage of crack initiation fatigue life increasing as the expansion size increases. The majority of the fatigue crack propagation life in CE specimens is concentrated in the initial stages of crack propagation. In addition, the effects of DCE and SCE processes on reducing the fatigue crack propagation rate are more pronounced along the thickness

direction compared to the width direction, leading to distinct crack propagation modes between CE and non-cold expansion (NCE) specimens.

Keywords: Hole Plates; Cold Expansion; Fatigue; Crack Initiation; Crack Propagation; FE; XFEM; CDM; TCD

1. Introduction

Cold expansion (CE) process (as show in Fig. 1(a)), which includes forcing an oversized mandrel going through the hole, is one of the most effective methods to increase the fatigue life of holed structures such as open-hole plates [1-3] and bolted joints [4-6]. Through the CE process, the fatigue life of structures can be increased without any extra weight gain, thus it is widely used in many industrial applications especially in aeronautical engineering [7-9]. Generally, the mechanisms of this process to increase the fatigue life is explained from two aspects: inducing the compressive residual stress around the hole edges [10-12] and refining the grains of the materials of the hole wall surfaces [13-15]. Nevertheless, this process exhibits several drawbacks. For instance, in some cases, the resistance force during the process can reach very high levels, leading to the fracture of the mandrel [16-18]. Additionally, the induced residual stress along the hole's axial direction is non-uniform, resulting in the mandrel entrance position becoming the weakest point where fatigue cracks tend to initiate [19-21]. These factors introduce challenges in conducting this process and impose limitations on the potential fatigue life enhancements. In recent years, researchers have proposed the Dynamic Cold Expansion (DCE) method (as illustrated in Fig. 1(b)) to address these drawbacks by considering the influence of mandrel speed on residual stress [22]. This approach has shown promising results, as demonstrated in previous studies [23-25]. The DCE process offers several advantages over the traditional static cold expansion (SCE) process. It effectively reduces the resistance force experienced during the process, resulting in an extended fatigue life compared to SCE. Furthermore, DCE induces larger compressive residual stress, particularly in the mandrel entrance layer, and contributes to more pronounced grain refinement when compared to SCE. The reasons why the DCE achieves better residual compressive stress can be seen in the reference [23-25]. First, aluminum alloy is hardened with the strain rate increment, which causes the yield strength of aluminum alloy increasing.

Therefore, larger residual compressive stress can be induced for the material during the DCE. Second, the residual stress is produced through the springback of the material after elastoplastic deformation. However, the mandrel decreases the springback of the hole wall surfaces of the material during SCE process since the duration of mandrel going through the hole is several seconds, much more than that in DCE process (only several milliseconds). These factors are considered the primary mechanisms responsible for enhancing the fatigue life in the DCE process.

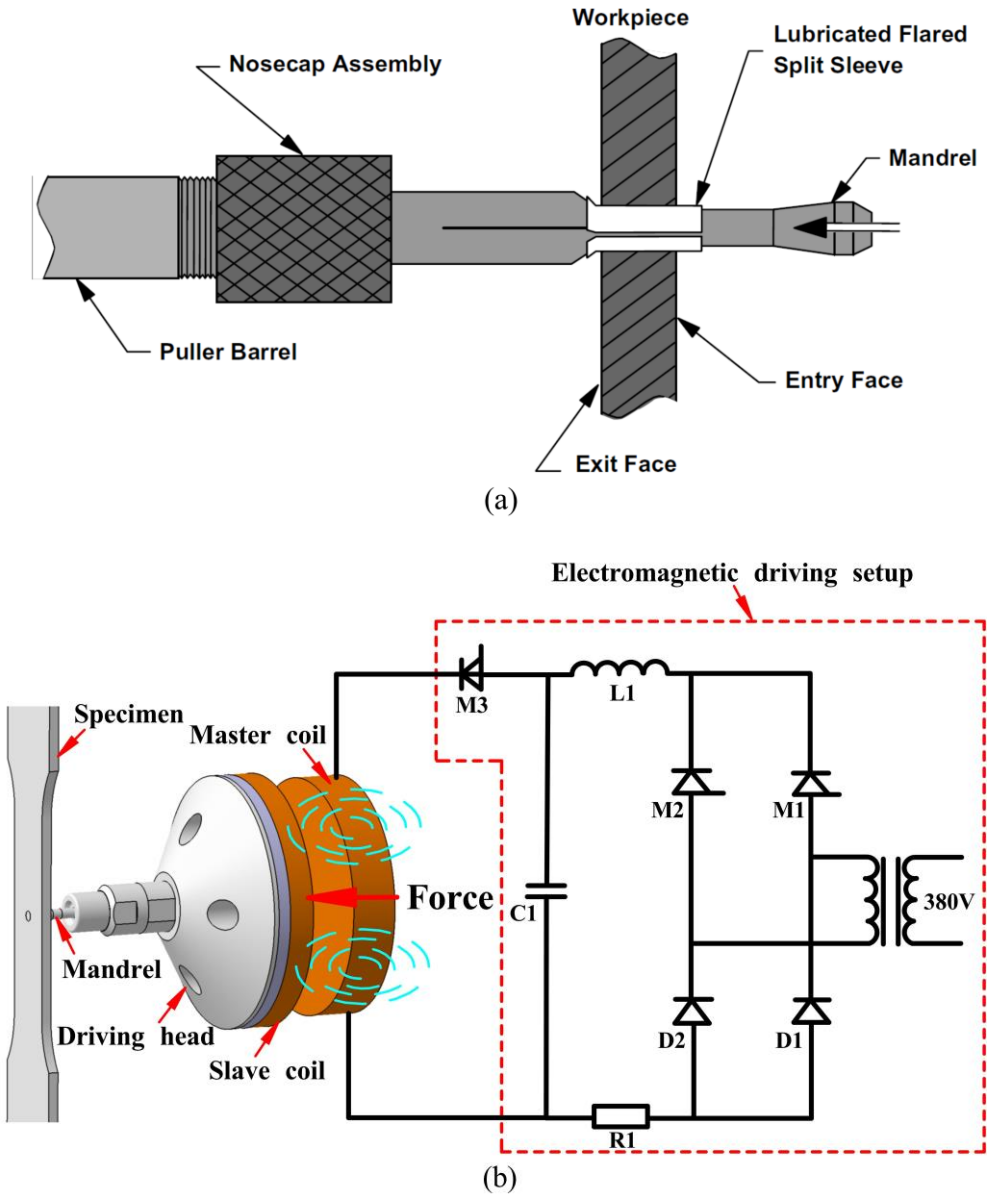

Fig. 1 The sketch of cold expansion process (a) The traditional SCE process [60] (b) The DCE process based on the electromagnetic load [24]

In general, conducting numerous tests to determine process parameters and estimate the final fatigue behaviors of Cold Expansion (CE) holes for various structures can be time-consuming.

Hence, the prediction of fatigue behaviors through Finite Element (FE) simulation is essential in engineering to reduce the number and cost of experiments. Additionally, simulation enables the identification of optimal process parameters that yield higher compressive residual stresses and longer fatigue lifetimes. The numerical estimation of fatigue behavior in CE specimens primarily involves two aspects: fatigue crack initiation [26-28] and fatigue crack propagation [29-31] lifetimes. Regarding fatigue life estimation, there are two common approaches: direct prediction of the total life [32-34] or separate prediction of fatigue crack initiation life and propagation life [35-36].

The hot-spot stress method has been utilized in several studies to incorporate the critical location of CE specimens for fatigue life prediction [37-39]. However, it is prone to significant errors in fatigue life estimation [40]. To overcome the limitations of the hot-spot method, the Theory of Critical Distance (TCD) has been introduced for predicting the fatigue life of CE specimens [41]. Liu et al. [9] combined TCD with the Smith-Watson-Topper (SWT) method to predict the fatigue life of aeroengine superalloy disk CE holes at elevated temperatures, obtaining good agreement with experimental results. However, their approach only considered stress along a single path, neglecting the stress distribution along the thickness direction, leading to inaccuracies in the results. Zheng et al. [24-25] considered stress distributions along the thickness based on the TCD method to predict the fatigue life of CE specimens and achieved favorable outcomes. Nevertheless, their proposed method did not account for fatigue crack propagation, thus lacking an investigation of the mechanisms behind fatigue crack propagation modes in CE specimens.

To predict the fatigue crack propagation behaviors, the commonly used approach is Linear Elastic Fracture Mechanics (LEFM), which assumes the material remains linearly elastic until failure and characterizes the fracture process with parameters such as stress intensity factor and energy release rate. LEFM has been employed to investigate fatigue crack propagation behavior in CE specimens, determining fatigue crack propagation life and paths [42-44]. These studies contribute to more reliable fatigue life prediction and enhance our understanding of fatigue crack propagation modes [45-47]. However, most published literature focuses on surface fatigue crack propagation at the mandrel entrance layer [48-50], neglecting crack propagation along the thickness direction. Although these approaches yield good agreement in two-dimensional fatigue

crack path prediction, they lack a comprehensive understanding of fatigue crack propagation modes, as the propagation modes in CE specimens differ from those in untreated fatigue specimens. Typically, fatigue crack lengths in Non-Cold Expansion (NCE) specimens are similar along the thickness direction, whereas in CE specimens, the crack length is much longer at the mandrel entrance layer than at the mandrel exit layer. The mechanisms underlying this phenomenon have not been thoroughly explained in previous works. Jones and Dunn [51] proposed a novel FE method that has considered through-thickness variation in residual stress to predict three-dimensional fatigue crack propagation in CE holes. The predicted crack propagation paths align well with the observed experimental results. Nonetheless, the predicted fatigue crack propagation life without considering residual stress relaxation was significantly greater than experimental data, while the results considering residual stress relaxation were conservative. This was because the equivalent stress at the smallest-section area was not comprehensively calculated to account for the non-uniform stress distribution in CE specimens. Furthermore, there is a lack of investigation into the fatigue crack propagation mechanisms for the novel DCE process. Therefore, developing a reliable method to predict fatigue behaviors, particularly fatigue crack propagation behaviors in both SCE and DCE specimens, is necessary.

This study introduces two methods for predicting the fatigue behaviors of CE open-hole plates, utilizing Continuum Damage Mechanics (CDM), the eXtended Finite Element Method (XFEM), and the Theory of Critical Distance (TCD). The first method focuses on predicting the total fatigue life, while the second method separately predicts fatigue crack initiation life and propagation life. In order to account for the non-uniform stress distributions in CE specimens, the Line Method (LM) is enhanced by introducing a novel parameter called CE affected distance. FE models are developed to simulate residual stress, stress under external cyclic loads, and fatigue propagation behaviors. Both methods are then evaluated, compared, and the study delves into the mechanisms behind fatigue life enhancements and fatigue crack propagation modes observed in CE specimens.

2. Theoretical background

This study introduces two methods, as illustrated in Fig. 2, to predict the fatigue life of CE

specimens. Method 1 focuses on directly predicting the total fatigue life. The total life S-N_f curve is fitted using the power law, based on plain fatigue testing data. Subsequently, the TCD is utilized to determine the equivalent stress σ_{eq} at the smallest cross-section area. To account for the residual stress induced by the CE process, a novel parameter called CE affected distance (L_a) is introduced, and an equivalent critical distance L_{eq} is defined. Finally, the total fatigue life (N_f) of the CE plates is obtained by utilizing the fitted S-N_f curve and calculating the equivalent stress σ_{eq}.

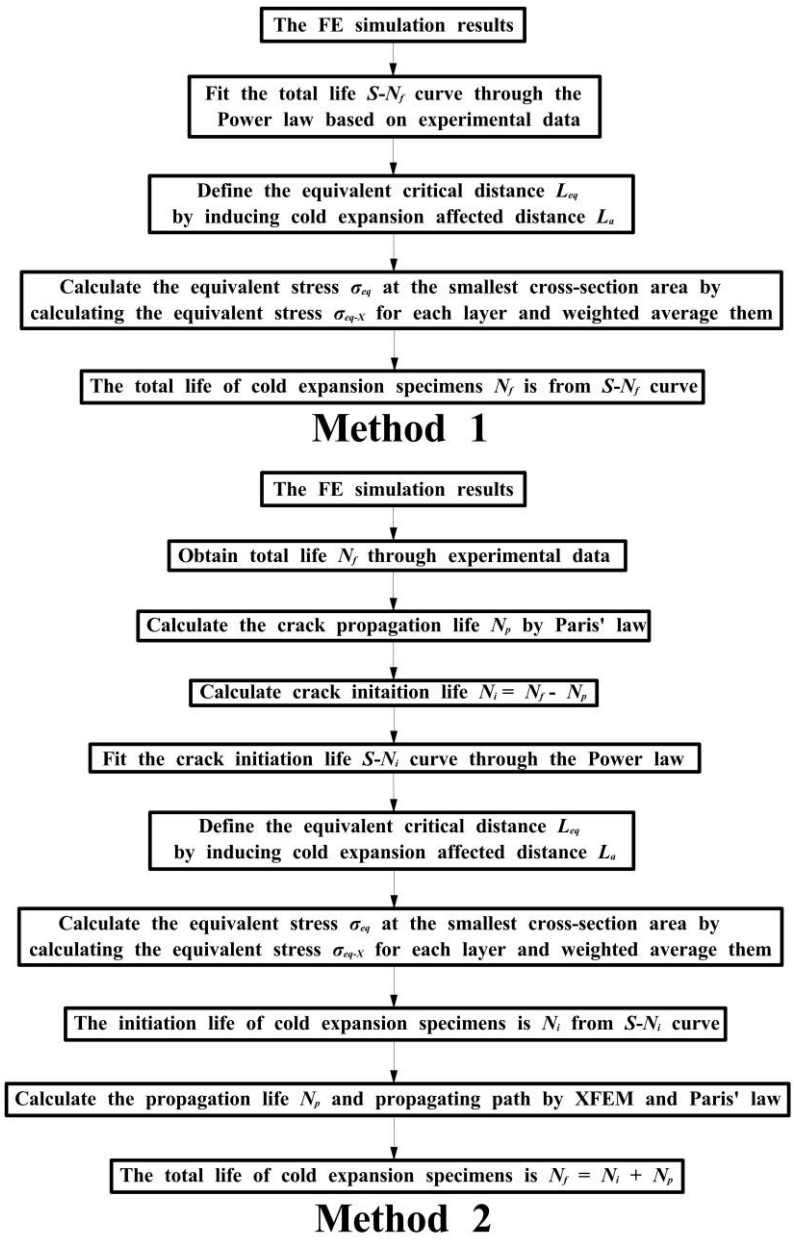

Fig. 2 Methods to predict the fatigue behaviors of open-hole plates treated by the CE

In Method 2, the prediction of fatigue crack initiation life and propagation life is carried out separately. It is important to note that in order to calibrate the material parameters for the total life

prediction, plain fatigue data was utilized, as they represent the overall fracture behavior. However, for the estimation of crack nucleation life, it becomes necessary to subtract the crack propagation life from the total lifetime and recalibrate the parameters specifically for crack initiation lifetime, where a crack length of 0.1mm is considered in this study. To achieve this, the propagation life of the plain specimens was estimated for all the data using Paris' law, enabling the subtraction of the propagation life from the total life. Subsequently, the fatigue crack propagation (N_p) of the open-hole plates is simulated using the extended finite element method (XFEM). Finally, the total life (N_f) can be calculated by summing up the crack initiation life (N_i) and the crack propagation life (N_p).

2.1 Continuum Damage Mechanics (CDM) approach

In this study, CDM is used to predict the fatigue life of open-hole plates treated by the CE process. This approach explains the material degradation when subjected to different loading conditions. To do so, a scaler damage parameter D is defined to address the effects of micro and macro scale damages on the mechanical response of materials, as follows:

$$D = \frac{\delta S_D}{\delta S} \tag{1}$$

where δS is the total area, δS_D is the damaged area. According to this, $D = 0$ corresponding to the undamaged state and $D = D_c$, corresponding to a fully damaged state, where D_c is a critical damage value and $D_c = 1$ here for simplification. Generally, the damage accumulation for high cycle fatigue which is suitable for this study is defined as [52]:

$$\frac{dD}{dN} = \left[\frac{\sigma_{eq}}{\sigma_r (1-D)} \right]^t \tag{2}$$

where the σ_r can be calculated as:

$$\sigma_r = \sigma_o \left(1 - k \frac{\sigma_m}{\sigma_u} \right) \tag{3}$$

where σ_{eq} denotes the equivalent stress of the maximum value of the cyclic stress, the σ_m and N are mean stress and the number of fatigue cycles to failure, σ_0, σ_u, k and t are all material constants, σ_r is resistance stress that resist against the fatigue damage accumulation [53], and is the function of

σ_m. When $D = D_c$, the equation (2) yields:

$$\int_0^N dN = \int_0^1 \left[\frac{\sigma_r (1-D)}{\sigma_{eq}} \right]^t dD \tag{4}$$

Then, fatigue life N and the equivalent stress σ_{eq} can be calculated as follows:

$$N = \frac{1}{1+t} \left(\frac{\sigma_r}{\sigma_{eq}} \right)^t \tag{5}$$

$$\sigma_{eq} = \frac{\sigma_r}{(1+t)^{\frac{1}{t}}} N^{-\frac{1}{t}} \tag{6}$$

The *S-N* curve for fatigue loading in form of power-law fit is defined as follows:

$$\sigma_{eq} = \sigma_f^{'} N^b \tag{7}$$

where $\sigma_f^{'}$, b are material constants. Combining the equations (5), (6) and (7), then:

$$t = -\frac{1}{b} \tag{8}$$

$$\sigma_r = \sigma_f^{'} \left(1 - \frac{1}{b} \right)^{-b} \tag{9}$$

In method 1, the S-N_f curve can be fitted through the equation (7) and plain fatigue testing data. In method 2, the total fatigue lifetime of a plain fatigue test normally consists of crack initiation step and propagation portion. Hence, the S-N_i curve should be fitted, and the analytical fatigue crack propagation life N_p of the plain fatigue tests should be calculated first as follows:

$$N_p = \sum \frac{\Delta a}{C \Delta K^m} \tag{10}$$

where Δa is the total crack incremental sizes and can be calculated as:

$$\Delta a = a - a_{in} \tag{11}$$

where a is the crack size, a_{in} is the initial crack size and set as 0.1 mm (two times as the average grain size) [54], ΔK can be calculated as follows:

$$\Delta K = \sigma_{\max} F \sqrt{\pi a} \tag{12}$$

where σ_{max} is the maximum value of the cyclic loads, F is the shape factor and can be estimated as follows [55]:

$$F = 0.265\left(1-\frac{a}{w}\right)^4 + \frac{0.857+0.265^{\frac{a}{w}}}{\left(1-\frac{a}{w}\right)^{\frac{3}{2}}} \tag{13}$$

where w is the width of the specimens. Through equation (10), the analytical fatigue crack propagation life N_p is estimated and the analytical fatigue crack initiation life N_i can be obtained:

$$N_i = N_f - N_p \tag{14}$$

Here, the total fatigue life (N_f) is obtained from the plain fatigue testing data. Subsequently, the S-N_i curve is fitted to recalibrate the material parameters, enabling accurate numerical prediction of the crack initiation lifetime.

2.2 Equivalent stress and critical distance

To predict fatigue life for the open-hole plates through the *S-N* curves, the equivalent stress at the smallest cross-section area of specimens should first be calculated. Here, the LM in the TCD, which is commonly used for notched or holed structures, is adopted for calculating the equivalent stress $\sigma_{eq\text{-}X}$ of one layer (shown in the Fig. 3(b)). The LM is defined as follows [41]:

$$\sigma_{eq-X} = \frac{1}{L_{eff}}\int_0^{L_{eff}} \sigma(r)dr \tag{15}$$

where L_{eq} denotes the equivalent critical distance and is defined for the NCE specimens as follows:

$$L_{eq} = 2L \tag{16}$$

where L denotes the critical distance, which is a material constant. However, equation (16) is not suitable for the CE specimen due presence of the induced residual stress. Fig. 3(a) illustrates the stress distributions around the hole edge, where σ_e, σ_t and S are the stress distribution under external loads without the CE, the residual stress distributions induced by the CE and the stress distributions under external loads with the CE, respectively. Generally, the distance 2L is much smaller than the distance from the hole edges to the residual stress zone edges, which would cause

large errors if the value of $2L$ is used as the equivalent critical distance L_{eq}. To consider the effects of residual stress on the fatigue life for the CE specimens, a novel parameter CE affected distance L_a is proposed and can be obtained from FE results. The boundary of the CE affected distance L_a is defined as the position beyond which the residual stress varies no more than 10% along the width direction. Therefore, for the CE specimens, L_{eq} is defined as:

$$L_{eq} = 2L + L_a \tag{17}$$

Furthermore, the inhomogeneity of stress distributions along the thickness direction for the CE specimens should also be considered. In this study, the smallest cross-section area is divided into five layers, as shown in Fig. 3(b). The equivalent stress $\sigma_{eq\text{-}X}$ of each layer will be calculated through the equation (15) and weighted averaged to obtain the equivalent stress σ_{eq}, as follows:

$$\sigma_{eq} = \eta_1\sigma_{eq-en} + \eta_2\sigma_{eq-u} + \eta_3\sigma_{eq-m} + \eta_4\sigma_{eq-l} + \eta_5\sigma_{eq-ex} \tag{18}$$

where $\sigma_{eq\text{-}en}$, $\sigma_{eq\text{-}u}$, $\sigma_{eq\text{-}m}$, $\sigma_{eq\text{-}l}$ and $\sigma_{eq\text{-}ex}$ denote the equivalent stress of the mandrel entrance layer, upper middle layer, middle layer, lower middle layer and exit layer, respectively. η_1, η_2, η_3, η_4 and η_5 are the weight factors for each layer, and defined as follows:

$$\eta_i = \frac{2^{n-i}}{2^n - 1} \tag{19}$$

where n = 5. Finally, the total fatigue life in Method 1 and the fatigue crack initiation life in Method 2 can be obtained through the S-N curves and the equivalent stress σ_{eq}.

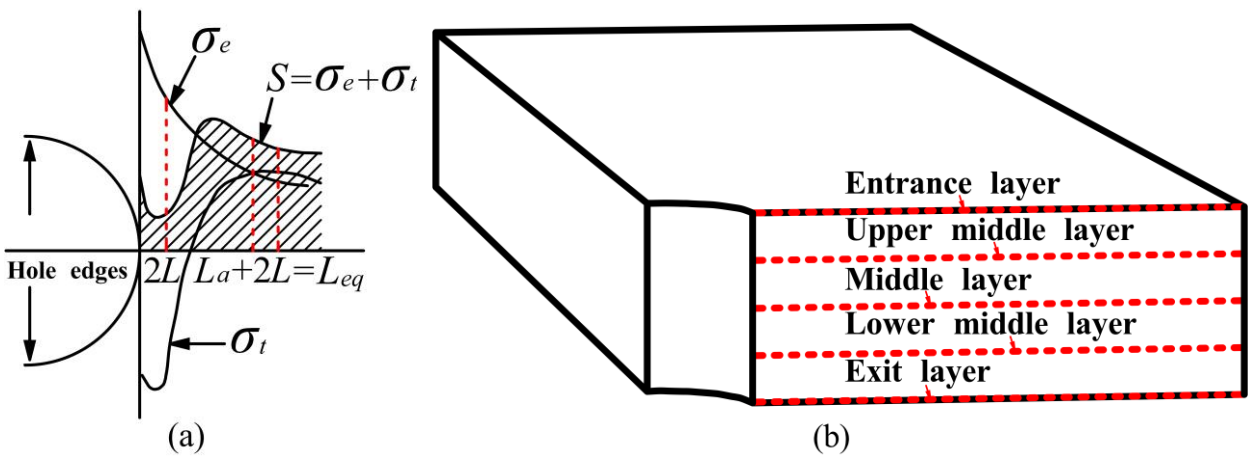

Fig. 3 Stress distributions around the hole edges and each layer to calculate the equivalent stress (a) Stress distributions around the hole edges (b) Each layer to calculate the equivalent stress σ_{eq}

2.3 Crack propagation lifetime

To numerically estimate the fatigue crack propagation life N_p, Paris' law which describes the crack growth rate is introduced:

$$\frac{da}{dN_p} = c_3 \Delta G^{c^4} \tag{20}$$

where c_3 and c_4 are the material constants, ΔG denotes the relative energy release rate and is defined as follows:

$$\Delta G = G_{\max} - G_{\min} \tag{21}$$

where $G_{\max}$ and $G_{\min}$ are the maximum and minimum value of energy release rate under one cycle of fatigue loads. Indeed, the material constants c_3 and c_4 are difficult to measure directly by experiments, thus here another form of Paris' law is introduced:

$$\frac{da}{dN_p} = C_k \Delta K^{m_k} \tag{22}$$

where ΔK is the stress intensity factor under one cycle of fatigue loads, C_k and m_k are material constants. For mode I crack, the relationship between the energy release rate G and the stress intensity factor K is:

$$G = \frac{K^2}{E_1} \tag{23}$$

where E_1 is the Young's modulus of materials. By combining equations (20), (21), (22) and (23) results in:

$$c_3 = C_k E_1^{\frac{m_k}{2}} \tag{24}$$

$$c_4 = \frac{m_k}{2} \tag{25}$$

Then c_3 and c_4 can be calculated by measuring the C_k and m, which are material constants, through experiments. Finally, the total life in method 2 is as follows:

$$N_f = N_i + N_p \tag{26}$$

To evaluate the accuracy of the proposed methods, error index E is defined:

$$E = \frac{N_{exp} - N_{num}}{N_{exp}} \times 100\% \tag{27}$$

where N_{exp}, N_{num} are experimental fatigue life and numerically predicted fatigue life, respectively. To evaluate the stability of the proposed methods, the variance of error index $Var(E)$ is also calculated, as follows:

$$Var(E) = \frac{\sum \left(\mu(E) - |E_i| \right)^2}{n_i} \tag{28}$$

where $\mu(E)$ is the average value of all predicted data, E_i denotes each predicted data, n_i is the total number of predicted data.

3. Experimental testing

The dimensions of the fatigue specimens and mandrels used in the experiments are illustrated in Fig. 4. The specimens in this study are made of aluminum alloy 6061-T6, which has a Young's modulus of 71 GPa, a Poisson's ratio of 0.33, and a yield strength of 324 MPa. The mandrels utilized are fabricated from 6Cr4W3Mo2VNb high-speed steel, with a Young's modulus of 210 GPa and a Poisson's ratio of 0.3. The chemical composition of aluminum alloy 6061-T6 is provided in Table 1.

Table 1 Percentage chemical composition of 6061-T6 aluminum alloy

Al	Si	Fe	Cu	Mn	Mg	Cr	Zn	Ti
Balance	0.65%	0.47%	0.25%	0.07%	1.03%	0.11%	0.14%	0.03%

The DCE process is performed using electromagnetic loading, with a mandrel speed set at 5 m/s. The SCE process, on the other hand, is conducted using the ETM104C electronic universal testing machine, with a mandrel speed set at 1.7×10^{-4} m/s. The Expansion Size (E_s) is varied by adjusting the diameter of the mandrel's working region (D_m) and is defined as follows:

$$E_s = \frac{D_m - d}{d} \tag{29}$$

where d denotes the diameter of the central hole in the specimens. Four different expansion sizes

1.5% (E1), 3.0% (E2), 4.5% (E3) and 6.0% (E4) are considered for both the DCE and SCE processes.

To fit the *S-N* curve and validate the prediction methods, a series of fatigue tests were conducted on both plain specimens and CE specimens at room temperature. The fatigue tests were performed under specific conditions with a stress ratio (*R*) of 0.1 and a frequency (f) of 10 Hz.

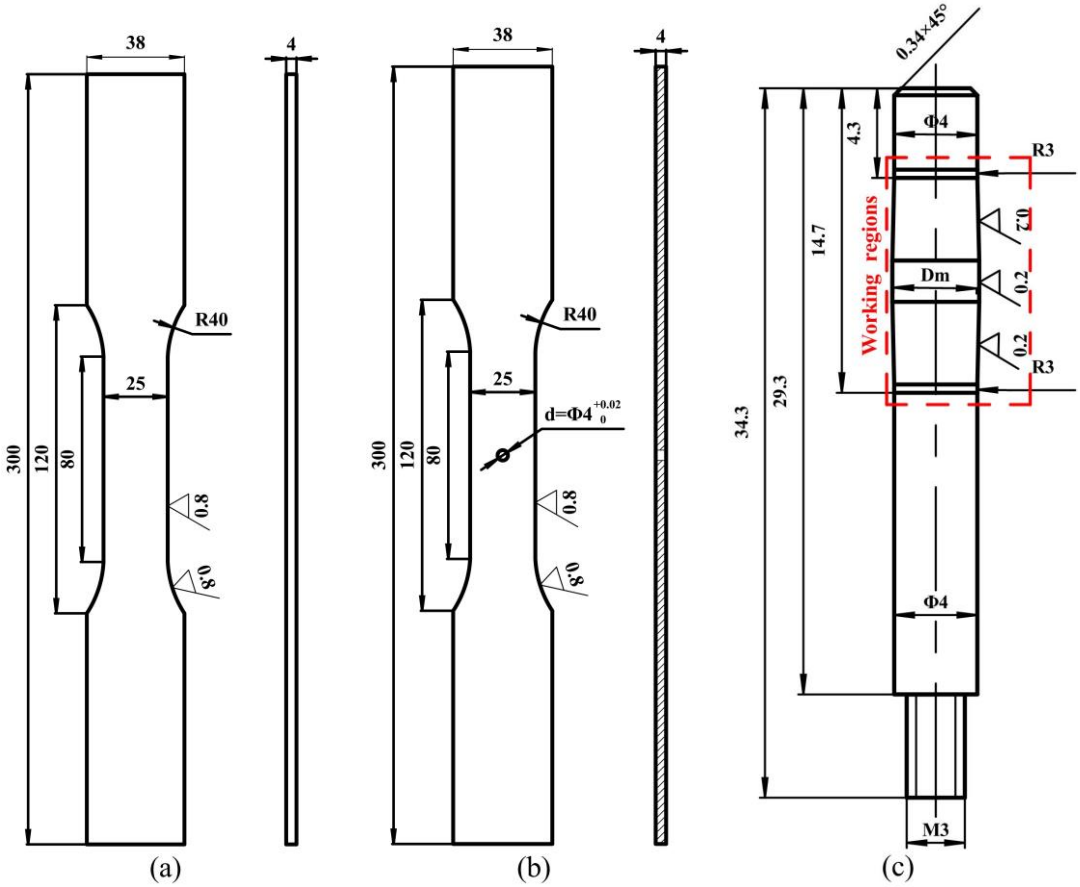

Fig. 4 Dimensions of the specimens and mandrel (a) Specimen for the plain fatigue tests (b) Specimen for the CE and the fatigue tests (c) Mandrel for the CE

For the plain fatigue tests, six different load levels were applied, with maximum stresses of 256 MPa, 238 MPa, 202 MPa, 156 MPa, 111 MPa, and 100 MPa. In the fatigue tests conducted on the CE specimens, three load levels were considered for each expansion size, with maximum stresses of 238 MPa (L3, approximately 73% of the yield strength), 202 MPa (L2, approximately 62% of the yield strength), and 156 MPa (L1, approximately 48% of the yield strength). Three repeated tests are conducted for each condition. These load levels were selected to cover a range of stress levels for the CE specimens. Additionally, corresponding tests were carried out on the NCE

specimens to serve as a comparison.

4. Numerical simulation

4.1 loading and boundary conditions

The simulation begins with the CE process to obtain the residual stress distributions and the CE affected distance (L_a), which is then utilized to calculate the equivalent critical distance L_{eq} using Equation (17) (the critical distance (L) is specified in Table 2). The results obtained from the CE simulation are then utilized as pre-field data for the fatigue model, where the cyclic load is applied.

Table 2 Some fatigue parameters of aluminum alloy 6061-T6 (Units *N* and mm)

Parameters	L [56]	C_k [59]	m_k [59]	c_3	c_4
Values	0.28	5.88×10^{-11}	2.57	1.11×10^{-4}	1.29

In the fatigue model, two distinct loads are applied to the plate. The first load consists of a single cycle of the cyclic load, simulating the stress distributions for calculating the total lifetime (N_f) in method 1 and the crack initiation life (N_i) in method 2. The second load corresponds to the cyclic load used to simulate crack propagation, enabling the calculation of the crack propagation life (N_p) in method 2.

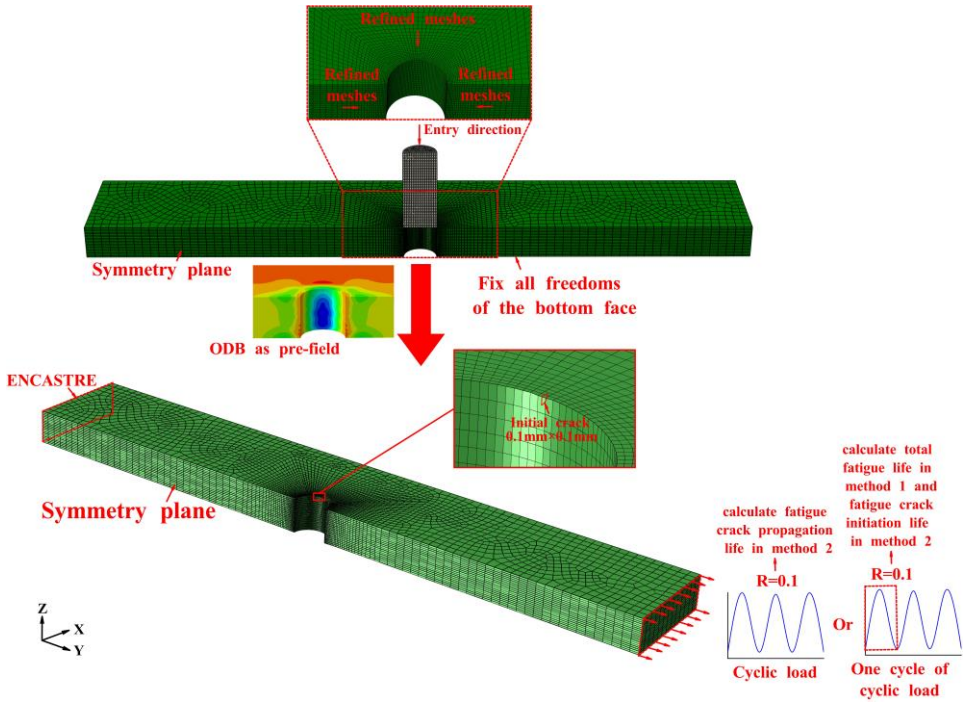

Fig. 5 FE models for CE process and external loading process

The FE models employed in this study are illustrated in Fig. 5. To minimize the computational time and optimize efficiency, a half model configuration is adopted. These FE models are developed using the ABAQUS software, utilizing C3D8R elements to ensure accurate representation of the structural behavior. The mesh refinement strategy focuses on enhancing resolution in proximity to the hole edges, with a minimum size of 0.05 mm × 0.05 mm at these critical regions. After the mesh converged analysis, the results are very similar between using the 0.05 mm × 0.05 mm meshes and the 0.02 mm × 0.02 mm meshes. Therefore, the minimum size used is chosen as 0.05 mm × 0.05 mm to simplify the simulation.

For the comprehensive simulation of the CE process, implicit, dynamic modeling technique is applied. The CE simulation entails fixing the bottom face of the plate while subjecting the mandrel to controlled displacement loading as it traverses the hole. The selected contact formulation is surface-to-surface, enabling accurate interaction between the mandrel and the hole wall surfaces. This contact model incorporates a friction coefficient of 0.1, consistent with relevant studies in the field [8, 18, 58]. In addition, the isotropic plasticity hardening model is used in the simulation of the CE cold expansion.

In the fatigue model used to estimate the crack initiation lifetime, boundary conditions involve fixing one side of the plate, while a single cycle of cyclic load is applied to the opposing side, effectively replicating the loading conditions employed in experimental investigations. In the crack propagation model, the XFEM is used to facilitate accurate representation of crack propagation phenomena. A crack with an initial size of 0.1 mm × 0.1 mm is positioned at the smallest cross-section area of the mandrel entrance layer, as visualized in Fig. 5. Subsequently, cyclic loads, consistent with the experimental setup, are applied to one side of the plate, while the opposing side remains fixed. Importantly, the parameters governing Paris' law, specific to aluminum 6061-T6, are meticulously defined and outlined in Table 2 [59].

4.2 Material constitutive models

In the simulation for the CE process and fatigue models, the Johnson-Cook model is used to consider the dynamic response of the material, and defined as follows:

$$\bar{\sigma} = \left[A + B\left(\bar{\varepsilon} \right)^{n} \right]\left[1 + C\ln\left(\frac{\dot{\bar{\varepsilon}}}{\dot{\bar{\varepsilon}}_0} \right) \right]\left[1 - \left(\frac{T_1 - T_{room}}{T_{melt} - T_{room}} \right)^{m} \right] \tag{30}$$

where $\bar{\sigma}$ is the equivalent flow stress, $\bar{\varepsilon}$, $\dot{\bar{\varepsilon}}$ and $\dot{\bar{\varepsilon}}_0$ are the plastic equivalent strain, equivalent strain rate and reference strain rate, respectively. T_1, T_{melt} and T_{room} are the actual temperature, melting temperature, and room temperature, respectively. *A*, *B*, *C*, *n* and *m* are material constants and denote the yield strength coefficient, hardening modulus, strain rate sensitivity coefficient, hardening coefficient, and thermal softening coefficient, respectively. The Johnson-Cook model parameters of aluminum alloy 6061-T6 are shown in Table 3 [57].

Table 3 Parameters of Johnson-Cook model for aluminum alloy 6061-T6 [57]

Parameters	*A*/MPa	*B*/MPa	*m*	*n*	*C*
Values	324	114	1.34	0.42	0.002

5 Results and discussions

5.1 Fatigue life prediction

The *S*-N_f curve is fitted through equations (7) along with the experimental data, as demonstrated in Fig. 6(a). Using Fig. 6(a), the total life N_f in method 1 can be obtained. In addition, the *S*-N_i curve is also fitted through the calculated results, as shown in Fig. 6(b). Using Fig. 6(b), the fatigue crack initiation life N_i in method 2 can be obtained.

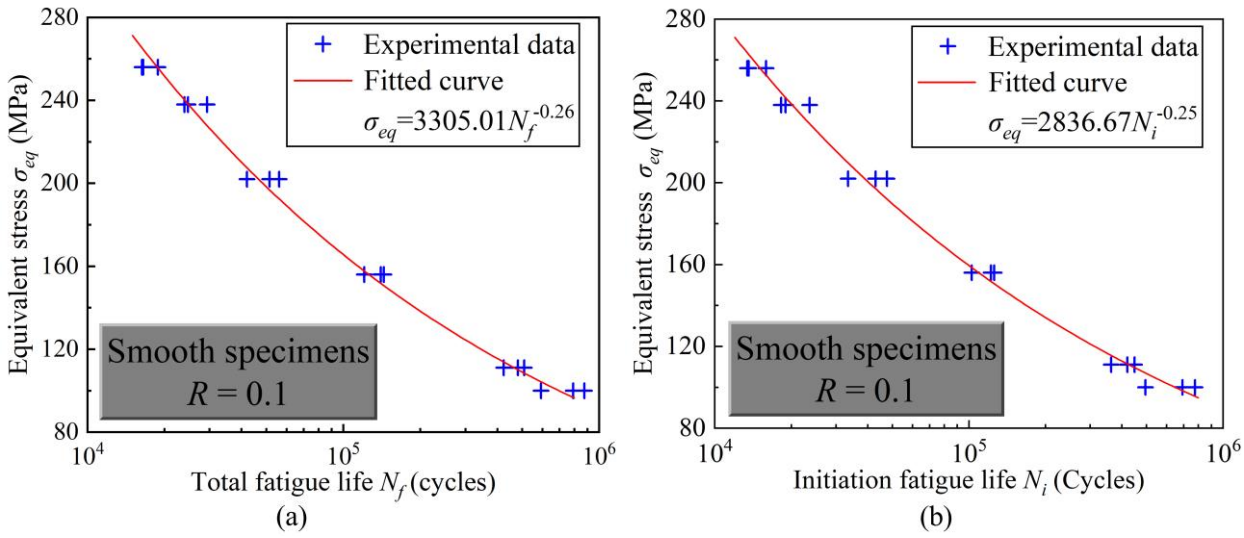

Fig. 6 Fitted *S*-*N* curves (a) Fitted *S*-N_f curve (b) Fitted *S*-N_i curve

What the external loads induce around the hole is mainly the tangential stress, and what causes the holed structures fracture is also the tangential stress. Therefore, it is widely accepted that the tangential stress is used to analyze and predict the fatigue life of the holed structures. In reference [9], the authors used the circumferential stress (tangential stress) to predict the fatigue life of aeroengine superalloy disk after the cold expansion. In reference [24, 25], the authors also used the tangential stress to predict the fatigue life of the cold expansion open-hole plates. Therefore, it is reasonable using the tangential stress to predict the fatigue life of holed structures. The simulated residual stress distributions of the CE specimens are shown in Fig. 7, and the CE affected distance L_a is marked in Fig. 7(a). It is clear that the L_a increases with the expansion size increasing. The value of L_a increases from 2.45mm to 4.28mm as the expansions size improves from E1 to E3 in the DCE specimens, which indicates that greater expansion size can contribute to larger residual stress zones. Moreover, the DCE process causes greater L_a under the same expansion size compared to the SCE process. The L_a of the DCE specimens are 2.45mm, 3.68mm and 4.28mm for E1, E2 and E3 expansion sizes, while those values of SCE specimens are 2.23mm, 3.43mm and 3.99mm, respectively. Using the CE affected distance L_a, the equivalent critical distance L_{eq} can be calculated by equation (17). Evidently, the trend of the L_{eq} is similar to that of the L_a.

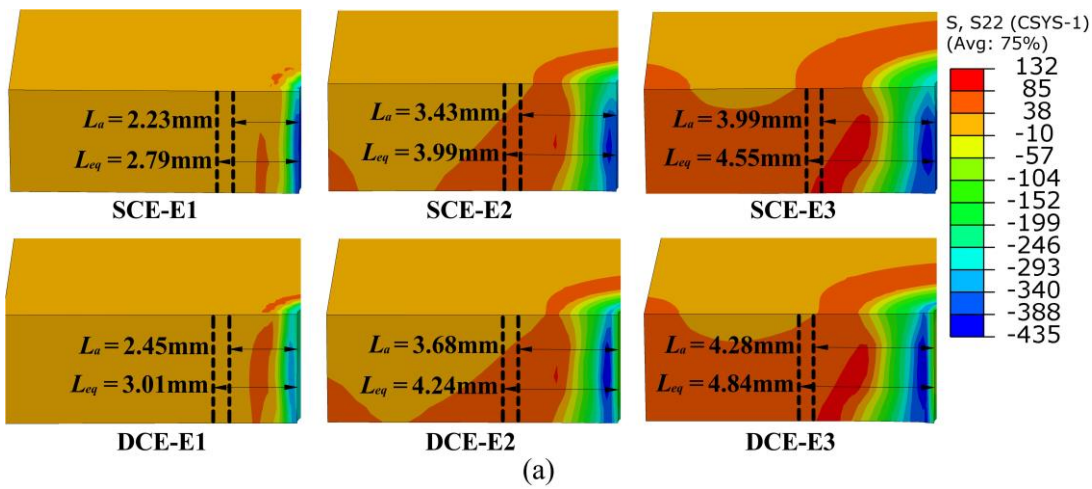

(a)

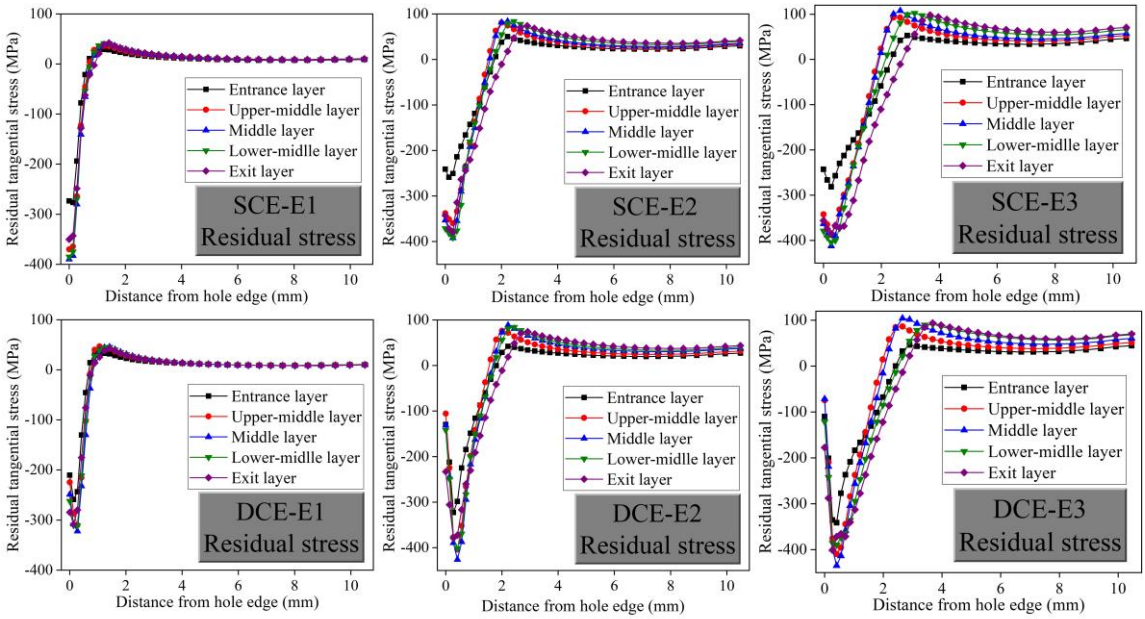

(b)

Fig. 7 Residual stress distributions at the smallest cross-section area under various expansion sizes (a) The counter map (b) The curves

The maximum tangential stress distributions under one cycle of the cyclic load are shown in Fig. 8. Fig. 8(a), (b) and (c) present the distributions under load level L1, L2 and L3, respectively. As illustrated in Fig. 8, the equivalent stress σ_{eq} reduces when the expansion size increases. Additionally, the equivalent stress σ_{eq} of the DCE specimens is lower than the SCE specimens under the same expansion size. Interestingly, when the expansion size increases from E3 to E4, the reduction of the equivalent stress in the SCE specimens is less significant than that in the DCE specimens. This may indicate that the DCE can achieve a larger expansion size upper limit, which in turn leads to higher fatigue life comparing with the SCE process.

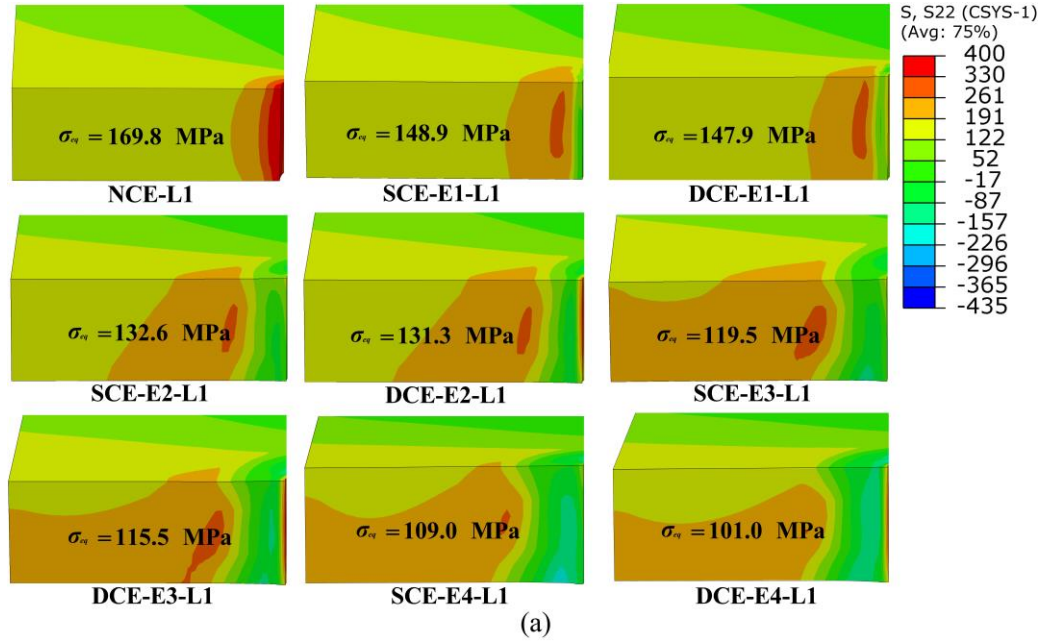
S, S22 (CSYS-1)
(Avg: 75%)
400
330
261
191
122
52
-17
-87
-157
-226
-296
-365
-435
σeq =169.8 MPa
NCE-L1
σeq =148.9 MPa
SCE-E1-L1
σeq =147.9 MPa
DCE-E1-L1
σeq =132.6 MPa
SCE-E2-L1
σeq =131.3 MPa
DCE-E2-L1
σeq =119.5 MPa
SCE-E3-L1
σeq =115.5 MPa
DCE-E3-L1
σeq =109.0 MPa
SCE-E4-L1
σeq =101.0 MPa
DCE-E4-L1

(a)

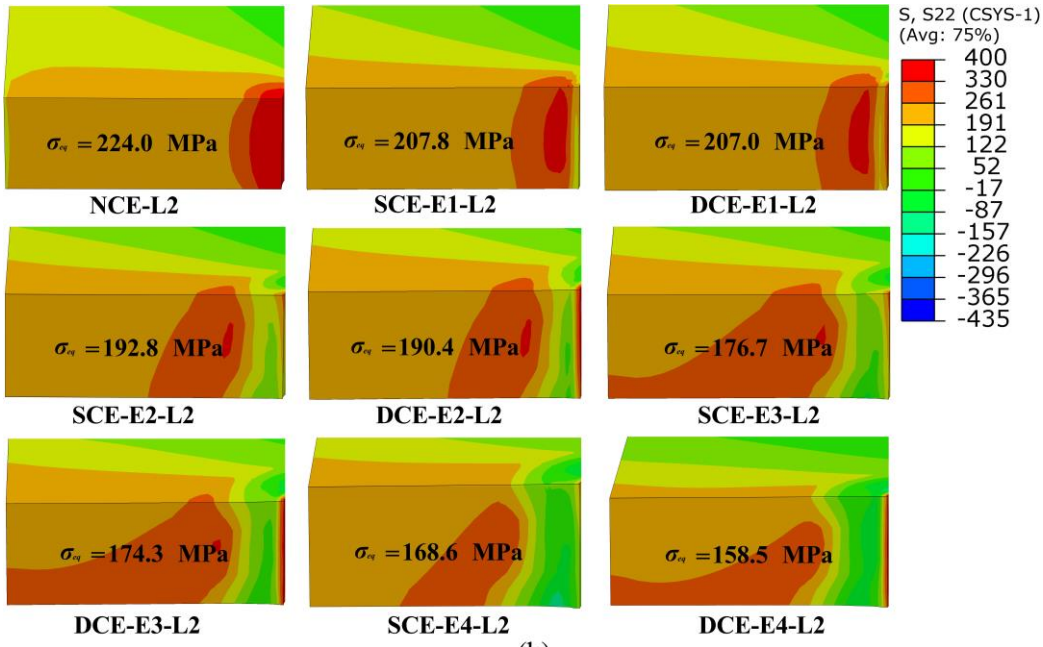
S, S22 (CSYS-1)
(Avg: 75%)
400
330
261
191
122
52
-17
-87
-157
-226
-296
-365
-435
σeq =224.0 MPa
NCE-L2
σeq =207.8 MPa
SCE-E1-L2
σeq =207.0 MPa
DCE-E1-L2
σeq =192.8 MPa
SCE-E2-L2
σeq =190.4 MPa
DCE-E2-L2
σeq =176.7 MPa
SCE-E3-L2
σeq =174.3 MPa
DCE-E3-L2
σeq =168.6 MPa
SCE-E4-L2
σeq =158.5 MPa
DCE-E4-L2

(b)

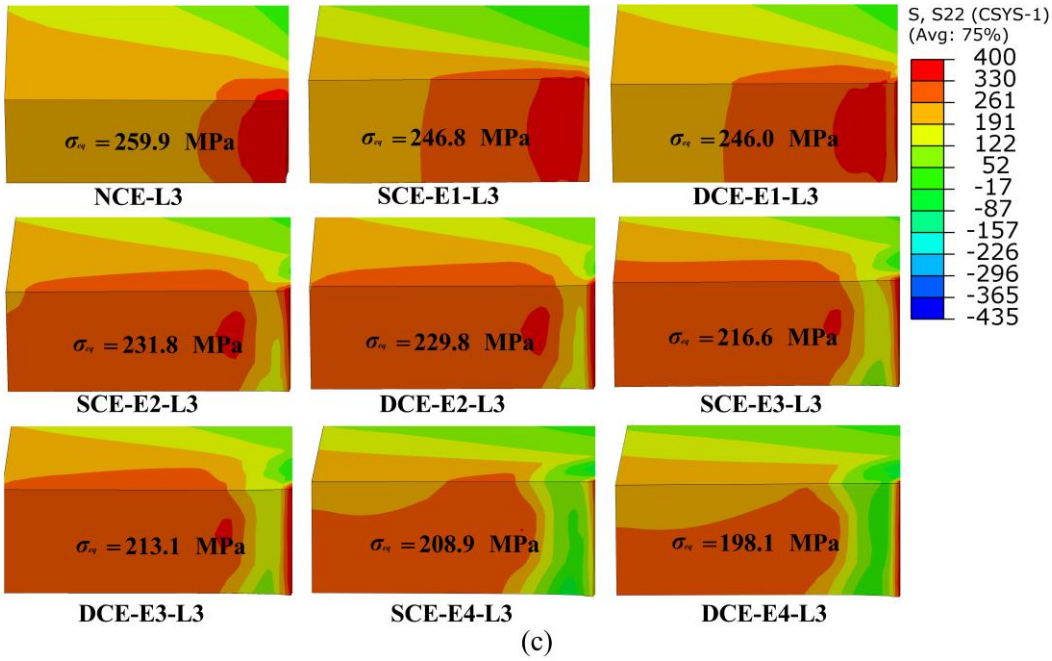

Fig. 8 Maximum stress distributions at the smallest cross-section area under one cycle of the cyclic loads for each condition (a) L1 load level (b) L2 load level (c) L3 load level

The precited fatigue lifetimes of NCE, SCE and DCE specimens using both method 1 and method 2 are presented in Fig. 9(a) to (f). From Fig. 9(a) and (b) it can be noticed that the obtained results of both methods show a good agreement with the observed experimental data (the average error index is within 30%). Moreover, the variance of the error index for both methods is very low, which indicates that they have good stability. However, method 2 has lower average and variance of error index than method 1. This is likely because that method 1 overestimates the fatigue crack propagation life, particularly for the large expansion size (E4) specimens. Generally, the CE process extends fatigue life via inducing the compressive residual stress, which has more effects on enhancing the crack initiation life than the crack propagation ones. Therefore, predicting the total life directly overestimates the fatigue crack propagation life of the CE specimens, especially under the large expansion size which induces the large compressive residual stress. The average and variance of the error index are acceptable if only considering the stress distributions of the mandrel entrance layer. However, it was found that without considering the CE affected distance the average error index is higher than 200% and the error index at some conditions is extremely high. Therefore, inducing the introduced novel CE affected distance parameter is essential to obtain reliable predictions.

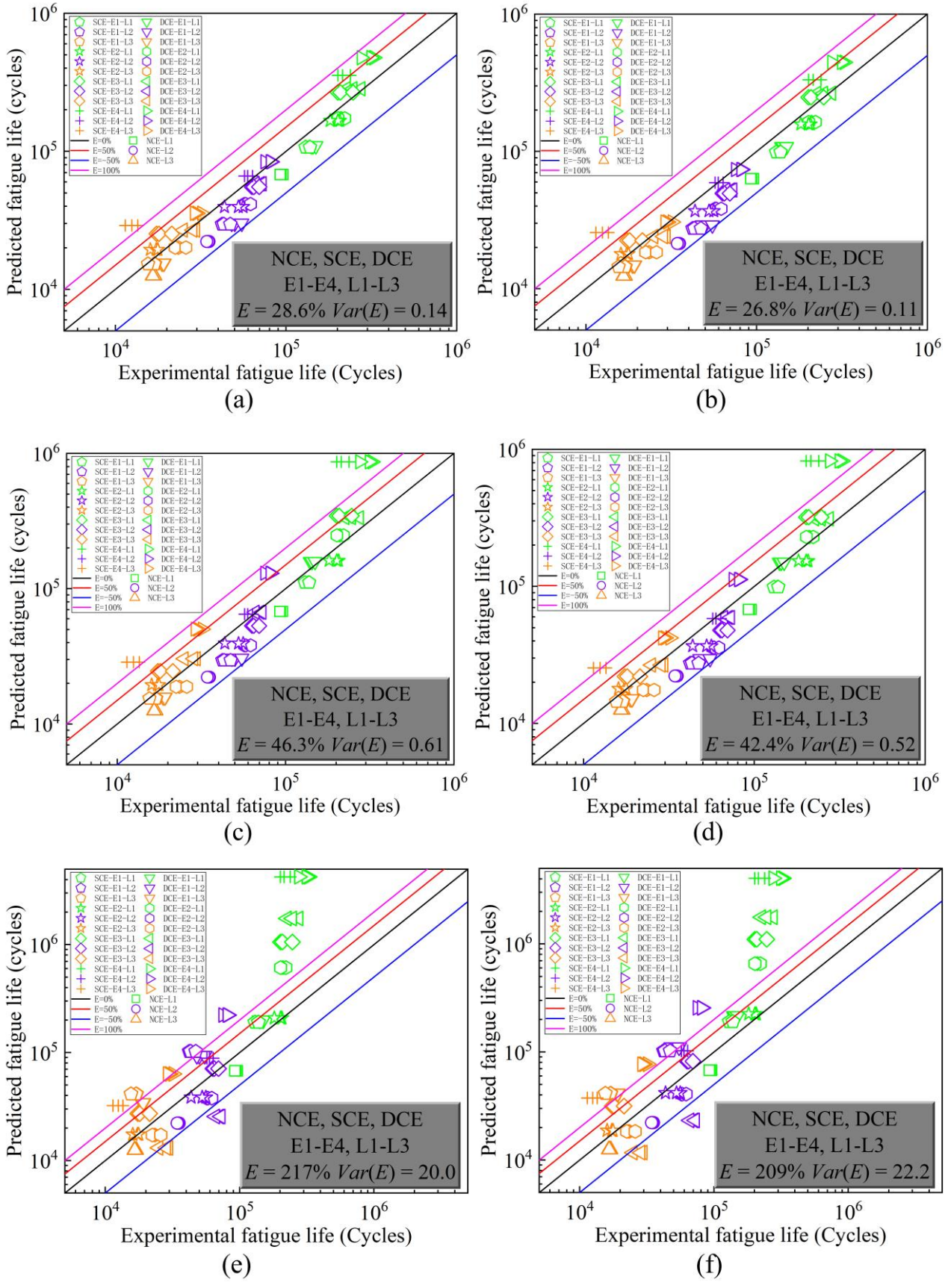

Fig. 9 Life prediction (a) Method 1 (b) Method 2 (c) Method 1 considering the entrance layer only (d) Method 2 considering the entrance layer only (e) Method 1 without L_a (f) Method 2 without L_a

5.2 Crack initiation and propagation lifetimes

The percentages of fatigue crack initiation and propagation lifetimes are demonstrated in Fig. 10(a) to (c). The results show that the fatigue crack initiation life forms the majority of the total fatigue life for both the NCE and CE specimens for all applied loading conditions. The percentage of fatigue crack initiation life occupies from 65% to 93% of the total life. Furthermore, the CE specimens, particularly the DCE specimens, have higher fatigue crack initiation life percentages compared to the NCE specimens, and the percentages increase with the improvement in the expansion size. For instance, under L3 load level, the percentage of fatigue crack initiation life of the NCE specimens is 65%, while the values of the DCE specimens are 68%, 73%, 77% and 81% for E1, E2, E3 and E4 expansion sizes. This indicates that the CE process extends fatigue crack initiation life more than crack propagation life, although both of them are prolonged.

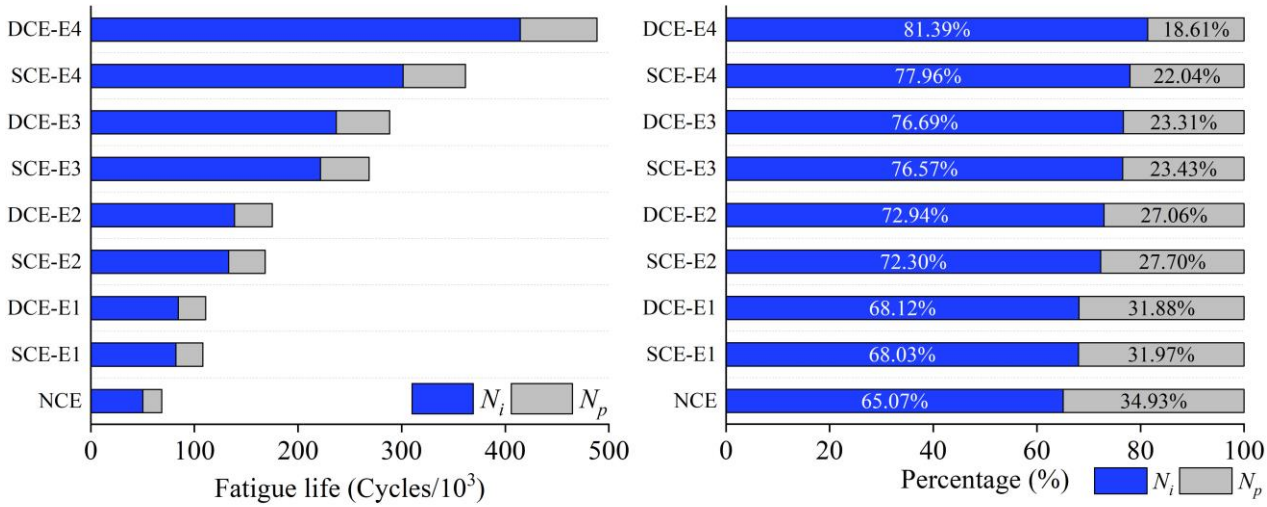

(a)

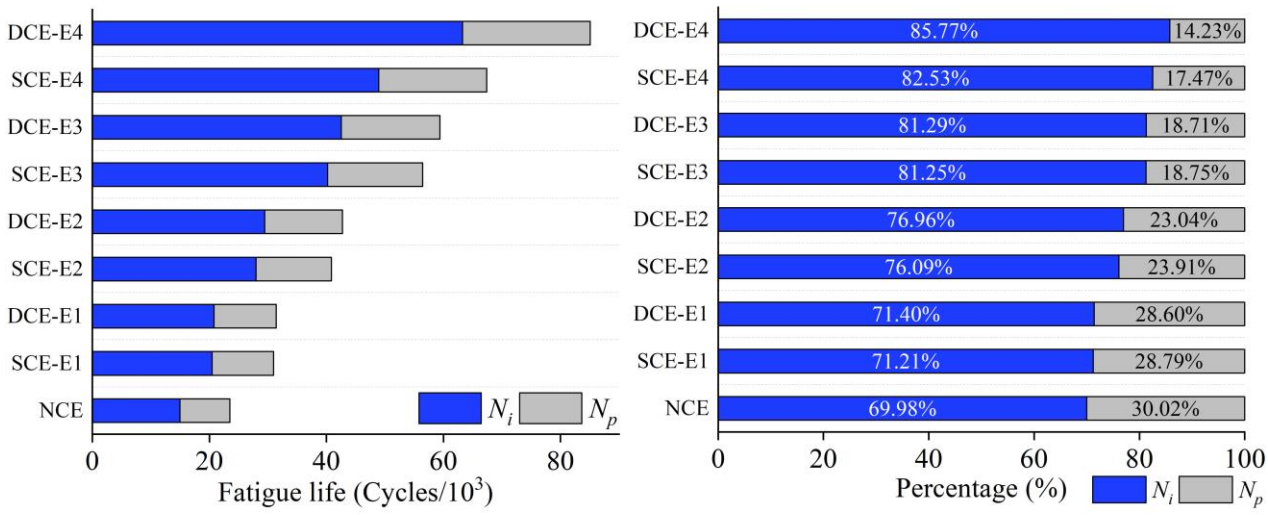

(b)

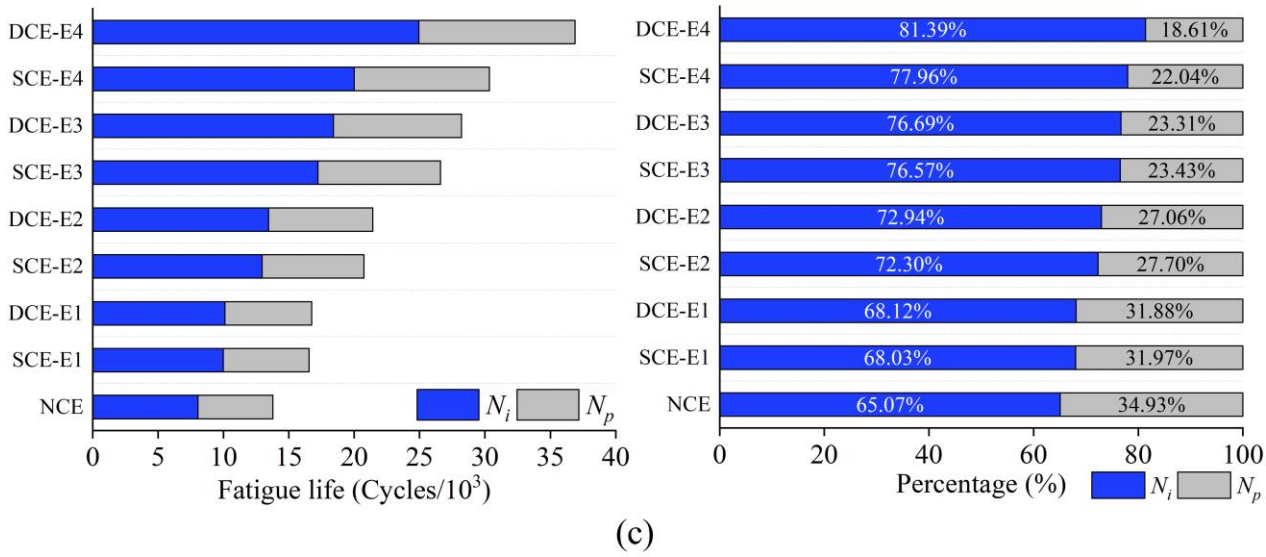

Fig. 10 Percentage of fatigue crack initiation and propagation life for each condition (a) Under L1 load level (b) Under L2 load level (c) Under L3 load level

This behavior may be attributed to two reasons. Firstly, as is known that the crack propagation rate is controlled by the stress intensity factor or energy release rate. When the initial crack starts to propagate, the compressive residual stress will be partially released. Under this condition, the compressive residual stress has limited effects on the stress distribution at the crack front and cannot significantly decrease the crack propagation rate as the fatigue crack advances. Secondly, there is tensile residual stresses at the locations beyond the compressive residual stress zone. Hence, the stresses at the crack front will be higher when the crack reaches these sites, which results in increasing the crack propagation rate and becoming detrimental for the crack propagation life. The aforementioned reasoning could also be used to understand why the method 2 (predict the total fatigue life separately) is superior to the method 1 (predict the total fatigue life directly).

5.3 Fatigue crack propagation

To verify the results of simulations, Fig. 11 shows the final fatigue crack propagation zones of both experiments and simulations under L1 load level for NCE specimen, SCE and DCE specimens with E4 expansion size. The observed and obtained results indicate that the shapes of final crack propagation zones are similar between the simulation and experiments. Moreover, the difference of crack length between the simulation and experiments for NCE, SCE and DCE specimens is only 0.8mm, 1.3mm and 1.0mm, respectively. These provide evidence that the

estimated simulations' results are reliable.

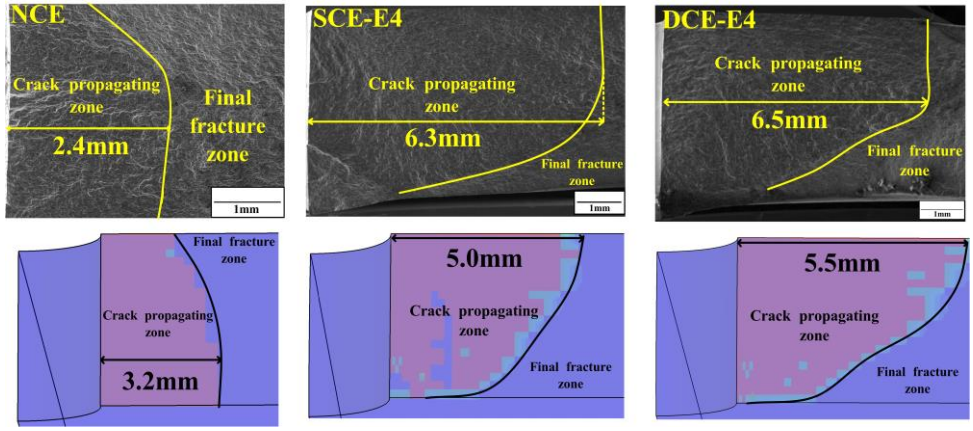

Fig. 11 The comparison of the final crack propagation between the experiments and the simulations under L1 load level

Fig. 12 illustrates the internal fatigue crack propagation progress of the DCE specimens under E4 expansion size and L1 load level. As Fig. 12 shown, the crack grows slowly at the beginning of the propagation progress. It grows from 0.1mm×0.1mm to 0.7mm×1.0mm at the first 19287 cycles. Then the crack grows very fast. It grows from 0.7mm×1.0mm to 5.5mm×4.0mm at the next 12002 cycles.

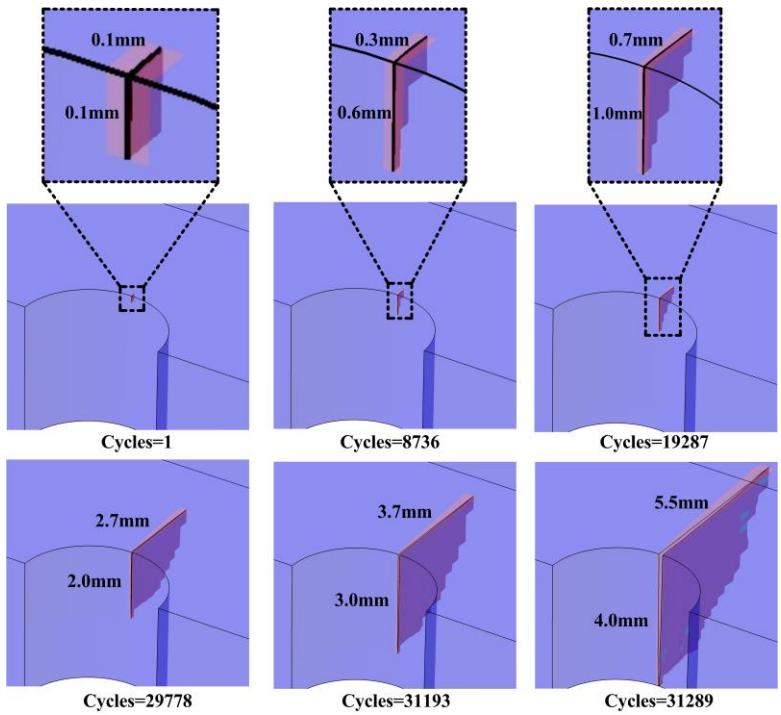

Fig. 12 The internal fatigue crack propagation paths of the DCE specimen under E4 expansion size and L1 load level.

Furthermore, Fig. 13 demonstrates the fatigue crack propagation of the specimens for simulated L1 loading conditions. It was observed that the CE processes, particularly the DCE process, can extend the fatigue crack propagation life as well as the fatigue crack propagation length along the width direction. As Fig. 14(a) shows, the stress at the fatigue crack front of the NCE specimens is very high, exceeding the ultimate strength of the material even at the beginning of the crack propagation, whereas that of the CE specimens is much lower due to the compressive residual stress at the beginning of the crack propagation (shown in Fig. 14(b)). This explains why the CE process can improve the fatigue crack propagation life.

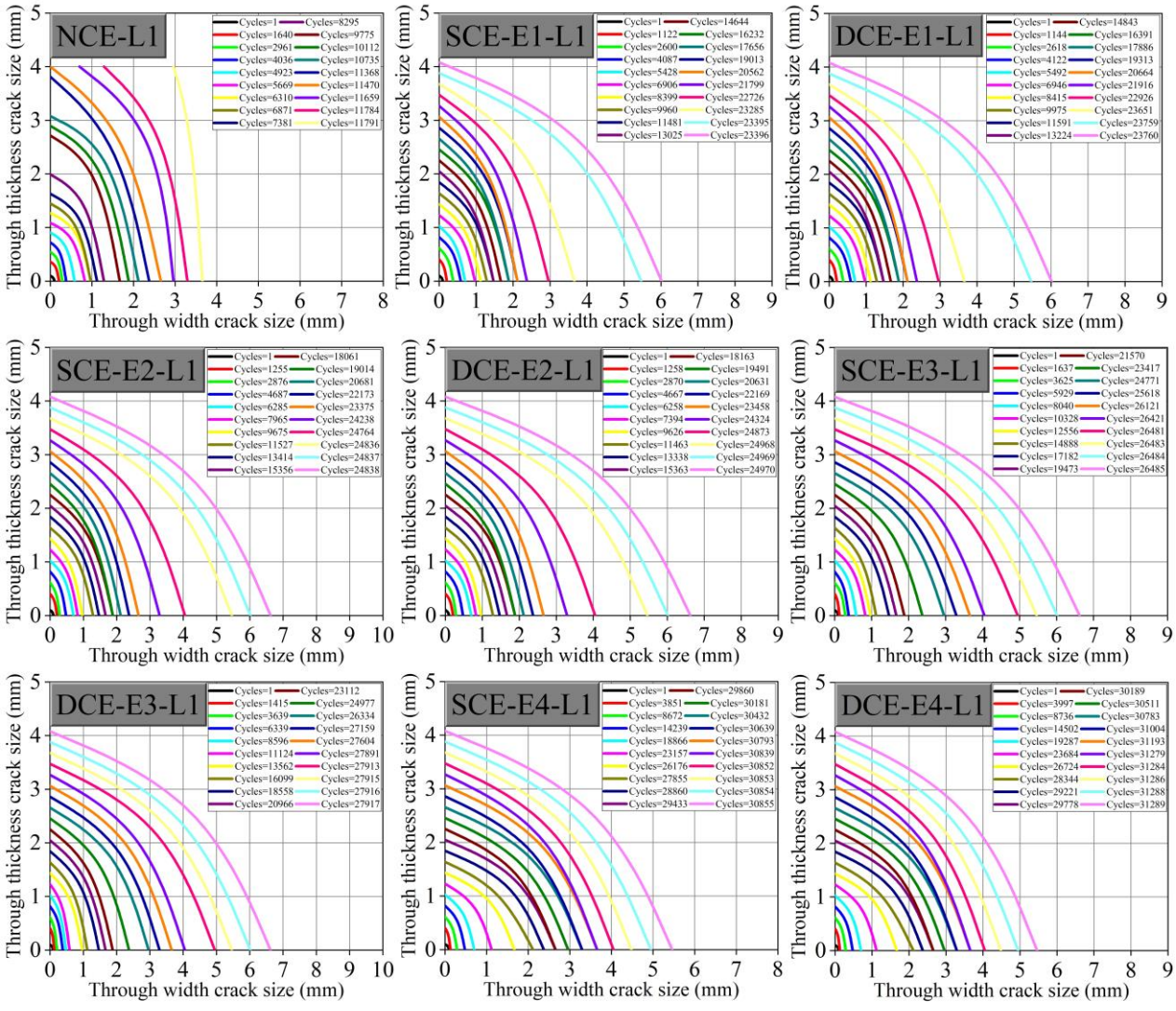

Fig. 13 Fatigue crack propagation paths for each condition under L1 load level

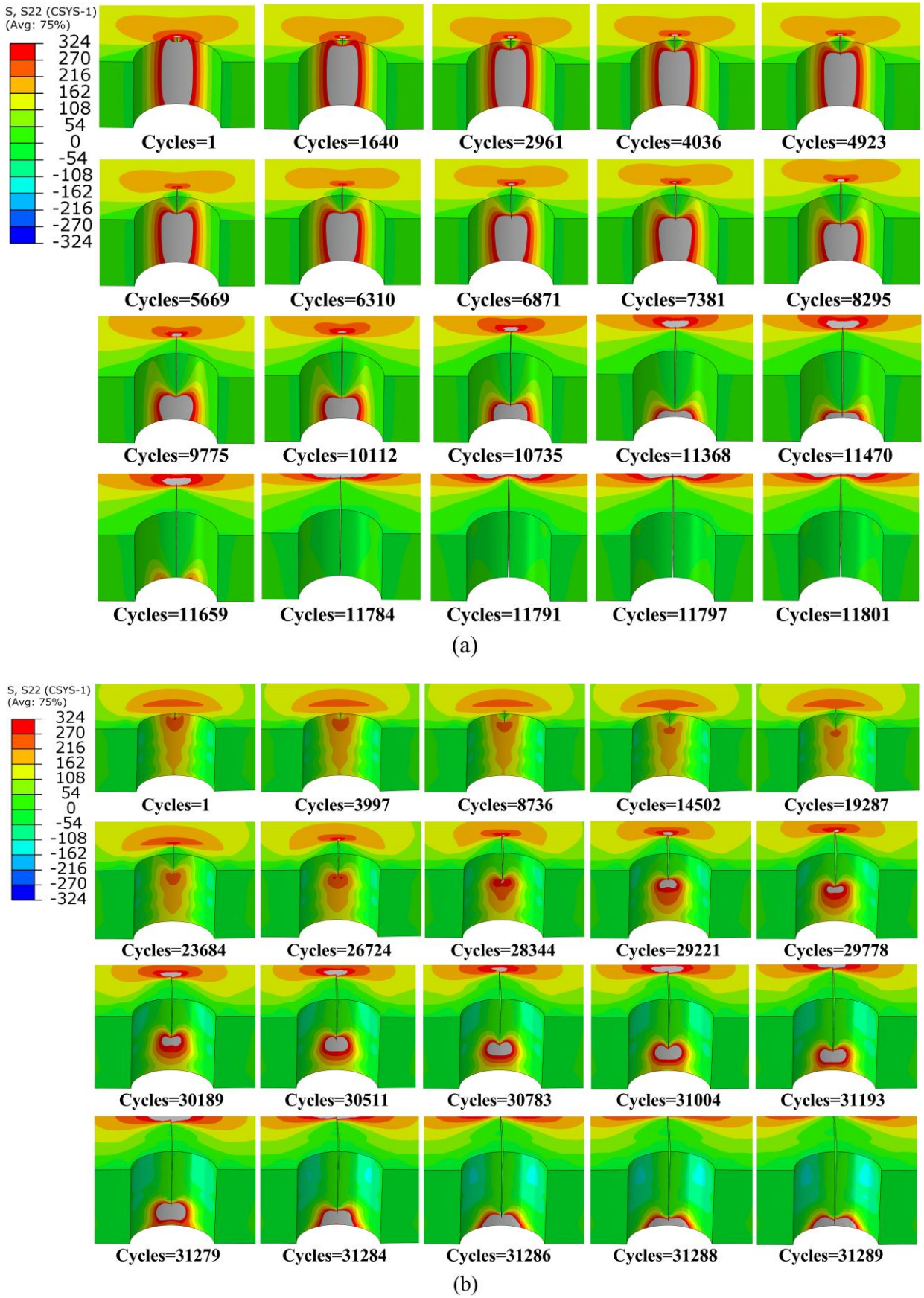

Fig. 14 The fatigue crack propagation paths under L1 load level (a) Propagation paths of the NCE specimen (b) Propagation paths of the DCE specimen under E4 expansions size

As shown in Fig. 11, 13, the crack shape during the crack propagation is different in the NCE and CE specimens. In the NCE specimens, the crack continues to propagate some distance along the width direction after it propagated through the full thickness. However, for the CE specimens, the fatigue crack stops propagating when or before it propagates through the full thickness. This phenomenon is evident in Fig. 15. The crack area of the CE specimens increases sharply at a particular point which can be considered as the number of cycles to fracture. The points also exist in the NCE specimens, yet the specimens still have some cycles before fracture. This may be due to the compressive residual stress induced by the CE, which has greater effects on decreasing the fatigue crack propagating rate on the thickness direction than the width direction.

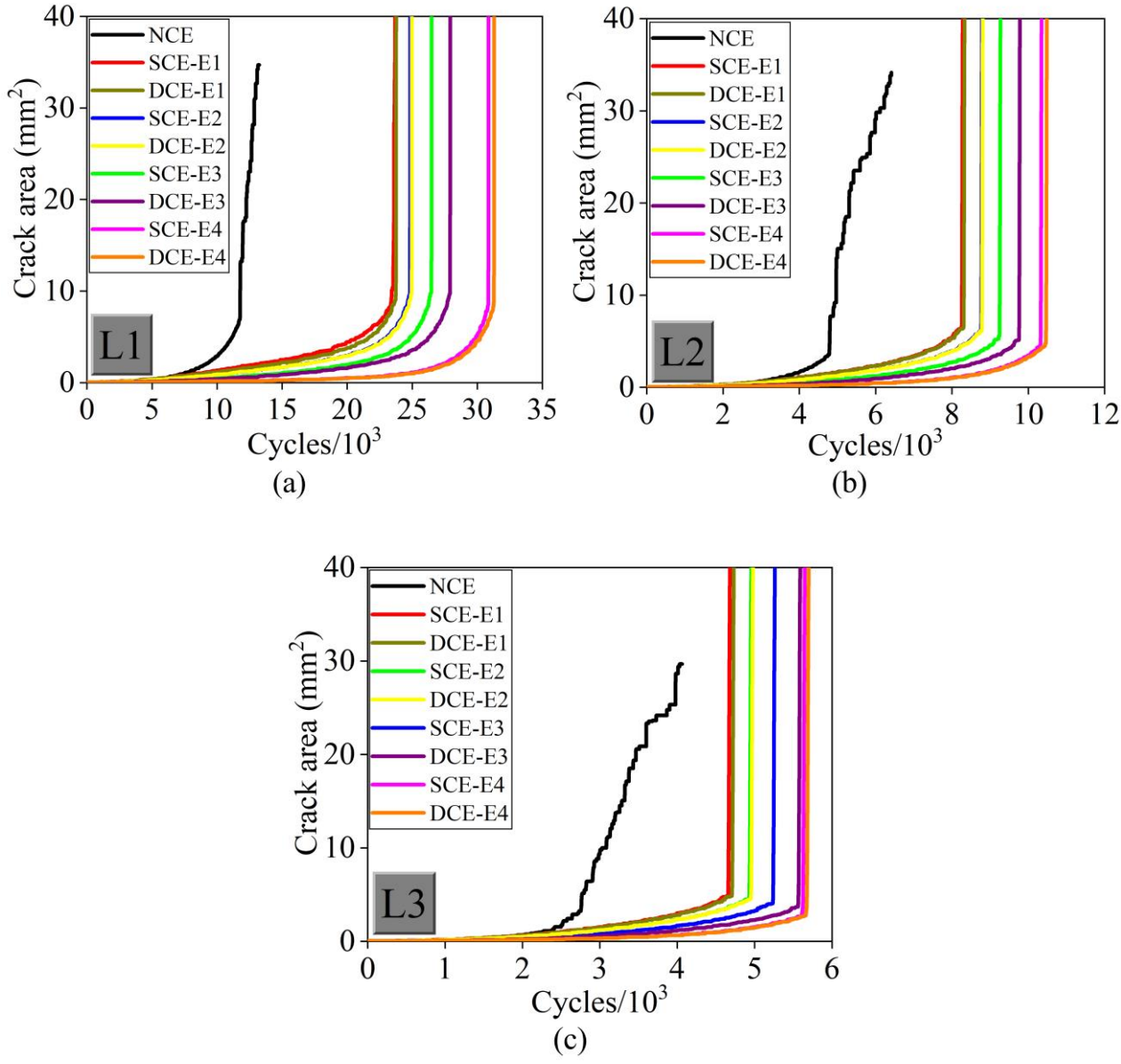

Fig. 15 Fatigue crack area varieties (a) L1 load level (b) L2 load level (c) L3 load level

Fig. 16(a) clearly show that the stress intensity factor and energy release rate at the fatigue crack front of the DCE specimens is consistently much lower than that of the NCE specimens along the thickness direction during the crack propagation. However, the differences are less pronounced along the width direction (as shown in Fig. 16(b)) as the crack propagates away from the hole edges beyond the compressive residual stress zone. It is suggested that the CE process is more effective to reduce the fatigue crack propagation rate along the thickness direction than the width direction, leading to a faster crack propagating along the width direction. Therefore, these differences in fatigue crack propagation behavior between the NCE and CE specimens can be attributed to the effects of the CE process (i.e. induced compressive residual stresses) on the crack propagation rate along the two directions.

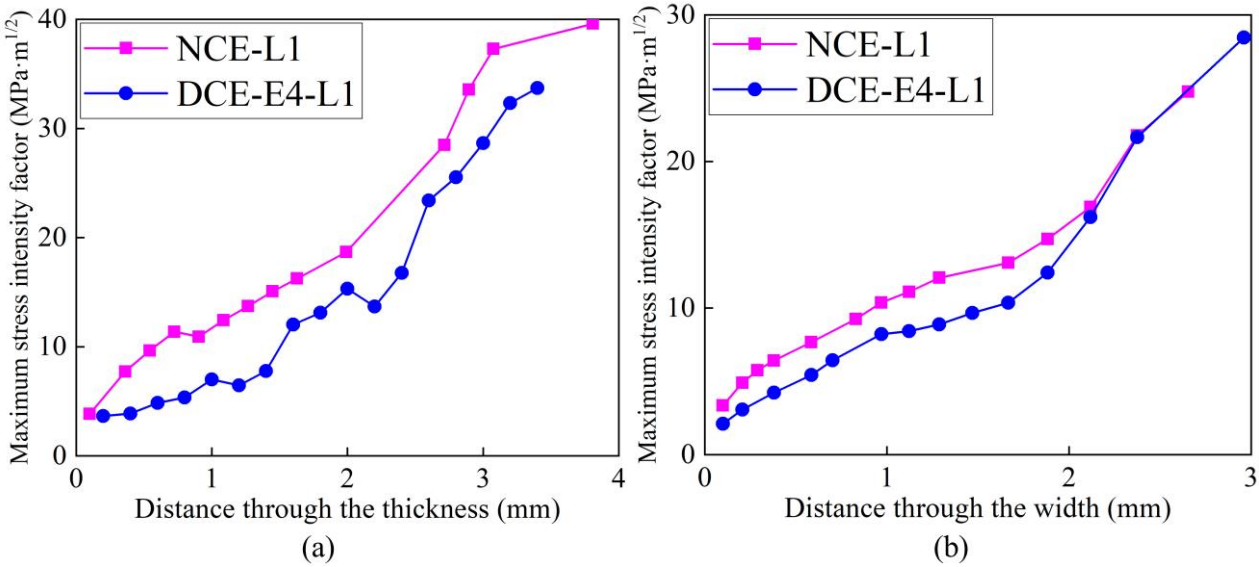

Fig. 16 The maximum stress intensity factor and energy release rate through the thickness and width directions at the fatigue crack tip (a) The maximum stress intensity factor through the thickness (b) The maximum stress intensity factor through the width

Additionally, the most effects of the CE process on the fatigue crack propagation occur at the beginning of the propagation progress, in which the propagation life occupies the majority of the total propagation life. This is because at the beginning stage of the fatigue crack propagation, the crack is small thus the compressive residual stress is not released much, and the crack is within the compressive residual stress zone. As a result, the governing stresses at the crack front are not very high (as shown in Fig. 14(b)). In this condition, the effects of compressive residual stress on

decreasing the crack propagation rate are significant. Nonetheless, as the crack advances, more of the compressive residual stress is released, and the crack exceeds the compressive residual stress zone, causing the stresses at the crack front to rise significantly (as shown in Fig. 14(b)). At this point, the effects of compressive residual stress on reducing the crack propagation rate begin to diminish. Therefore, the influence of the CE process on fatigue crack propagation life gradually decreases and it is less pronounced with the crack size increment.

6 Conclusions

In this study, two numerical methods based on the CDM, TCD and XFEM are proposed to predict the fatigue behaviors of open-hole plates treated by both the DCE and SCE processes. One is to predict the total lifetime directly, and another is to predict the fatigue crack initiation and propagation life separately. The S-N_f and S-N_i curves are fitted through the CDM and power law based on the experimental data, and the LM in the TCD is modified to be suitable for the CE specimens. Moreover, the developed FE models have been used to calculate the total fatigue life, crack initiation and the crack propagation. The corresponding fatigue testing is conducted to verify the developed models. Based on the observed experimental results and obtained numerical simulations, the following conclusions can be drawn:

1. The results of both methods used to predict the fatigue behaviors of the CE specimens show good agreement with the experimental data. Method 2, which predicts the fatigue life through dividing the total fatigue life into the fatigue crack initiation life and propagation life achieve lower average and variance of the error index than method 1which predicts the total fatigue life directly. This is because method 1 overestimates the effects of the CE process on the fatigue crack propagation life, particularly under the large expansion sizes.
2. The CE process, particularly the DCE process, can extend both of the fatigue crack initiation and propagation lifetimes, with more noticeable lifetime prolongation for the crack initiation part. Furthermore, the percentage of fatigue crack initiation life becomes larger with the expansion size increasing from 1.5% to 6%, indicating that the compressive residual stress induced by the CE process mainly affects the fatigue crack initiation life for the open-hole plates.

3. The CE process achieves more pronounced effects on reducing the fatigue crack propagation rate along the thickness direction than the width direction. This results in the differences of fatigue crack propagation response between the CE and NCE specimens. For the NCE specimens, the crack continues to propagate some distance along the width direction when it advances through the full thickness. However, the crack propagation of the CE specimens stops when or before propagating through the full thickness as the crack has propagated long distance along the width direction at this condition and even beyond the compressive residual stress zone, causing the extremely high stress distributions at the crack front.
4. The compressive residual stress induced by CE processes, especially the DCE process, primarily decreases the fatigue crack propagation rate at the beginning of the crack propagation. This is due to the compressive residual stress being partially released and even the crack exceeding the compressive residual stress zone as the crack length increases. Under this condition, the stresses at the crack front become extremely high leading to a sharp increase in the crack propagation rate.

Acknowledgement

The authors gratefully acknowledge the financial support from the China Scholarship Council (202106290066).

References

[1] Liu J, Shao XJ, Liu YS, Yue ZF. Effect of cold expansion on fatigue performance of open holes. Mater Sci Eng A 2008; 477(1-2): 271-6.

[2] Karabin ME, Barlat F, Schultz RW. Numerical and experimental study of the cold expansion process in 7085 plate using a modified split sleeve. J Mater Process Technol 2007; 189: 45-57.

[3] Sun Y, Hu W, Shen F, Meng Q, Xu Y. Numerical simulations of the fatigue damage evolution at a fastener hole treated by cold expansion or with interference fit pin. Int J Mech Sci 2016; 107: 188–200.

[4] Chakherlou TN, Vogwell J. A novel method of cold expansion which creates near-uniform compressive tangential residual stress around a fastener hole. Fatigue Fract Eng Mater Struct 2003;

27: 343-51.

[5] Geiglou Z, Chakherlou TN. Investigating the effect of cold expansion process on the fatigue behavior of aluminum alloy 7075-T6 in double-lap shear joints. P I Mech Eng L-J Mat 2018; 233(8): 1645-1660.

[6] Abdul KS, Xiang Z, James E, Robert M, Luigi C, Michael E. Fatigue performance of bonded crack retarders in the presence of cold worked holes and interference-fit fasteners. Int J Fatigue 2017; 105: 111-118.

[7] Fu Y, Ge E, Su H, Xu J, Li R. Cold expansion technology of connection holes in

aircraft structures: a review and prospect. Chinese J Aeronaut 2015; 28(4): 961-73.

[8] Rahman S. Total fatigue lives, crack growth paths and cycles in cold expanded adjacent holes. Int J Fatigue 2018; 119: 69-77.

[9] Liu H, Hua D, Wanga R, Wang X, Jin S, Gu Y. Experimental and numerical investigations on the influence of cold expansion on low cycle fatigue life of bolt holes in aeroengine superalloy disk at elevated temperature. Int J Fatigue 2020; 132: 105390.

[10] Semari Z, Aid A, Benhamena A, Amrouche A, Benguediab M, Sadok A, Benseddiq N. Effect of residual stresses induced by cold expansion on the crack growth in 6082 aluminum alloy. Eng Fract Mech 2013; 99: 159-168.

[11] Gopalakrishna HD, Narasimha Murthy HN, Krishna M, Vinod MS, Suresh AV. Cold expansion of holes and resulting fatigue life enhancement and residual stresses in Al 2024 T3 alloy – An experimental study. Eng Fail Anal 2010; 99: 361-368.

[12] Maximov JT, Duncheva GV, Amudjev IM, Anchev AP, Ganev N. A new approach for pre-stressing of rail-end-bolt holes. P I Mech Eng C-J Mec 2017; 231(12): 2275-2283.

[13] Faghih S, Shaha SK, Behravesh SB, Jahed H. Split sleeve cold expansion of AZ31B sheet: Microstructure, texture and residual stress. Mater Des 2020; 186: 108213.

[14] Gong P, Zheng LB, Zhang K. Effects of hole cold expansion on microstructure and fatigue property of 7B50-T7451 aluminum alloy plate. J Aeronaut Mater 2011; 31: 45-50.

[15] Wang X, Xu C, Chen X, Hu D, Hu B, Hu R, Gu Y, Tang Z. Effect of cold expansion on high-temperature low-cycle fatigue performance of the nickel-based superalloy hole structure. Int J Fatigue. 2021; 151: 106377.

[16] Liu Y, Shao X, Liu J, et al. Finite element method and experimental investigation on the residual stress fields and fatigue performance of cold expansion hole. Mater Des 2010; 31: 1208-1215.

[17] Shamdani AH and Khoddam S. A comparative numerical study of combined cold expansion and local torsion on fastener holes. Fatigue Fract Eng Mater Struct 2012; 35: 918-928.

[18]Liu Y, Liu J and Shao X. Study on the Residual Stress Fields, Surface Quality, and Fatigue Performance of Cold Expansion Hole. Mater Manuf Process 2011; 26: 294-303.

[19]Yanishevsky M, Li G, Shi G, et al. Fractographic examination of coupons representing aircraft structural joints with and without hole cold expansion. Eng Fail Anal 2013; 30: 74-90.

[20]Wang Y, Zhu Y, Hou S, et al. Investigation on fatigue performance of cold expansion holes of 6061-T6 aluminum alloy. Int J Fatigue 2017; 95: 216-228.

[21]Chakherlou TN, Shahriary P and Akbari A. Experimental and numerical investigation on the fretting fatigue behavior of cold expanded Al-alloy 2024-T3 plates. Eng Fail Anal 2021; 123: 105324.

[22] Farhangdoost K, Hosseini A. The effect of mandrel speed upon the residual stress distribution around cold expanded hole. Procedia Eng 2011; 10: 2184-2189.

[23] Zheng G, Cao Z and Zuo Y. A dynamic cold expansion method to improve fatigue performance of holed structures based on electromagnetic load. Int J Fatigue 2021; 148: 106253.

[24] Zheng G, Cao Z and Zuo Y. Fatigue life enhancement mechanism and lifetime prediction of AA6061-T6 open-holed sheet treated by electromagnetic driving dynamic cold expansion. Mater Today Commun 2022; 33: 104841.

[25] Zheng G, Cao Z Zuo Y, et al. Residual stress distribution and fatigue performance investigations of electromagnetic force-based dynamic cold expansion open-holed sheet. Proc IMechE Part L: J Materials: Design and Applications 2022; 237(5): 1109-1123.

[26] Li K, Wang R, Zhang X, Ya S, Cheng L, Lei X, Tu S. Process-performance-prediction integration for fatigue life improvement technologies: An implementation in cold expansion of hole structures. Int J Fatigue 2023; 170: 107507.

[27] Mostefaa B, Abdelkrima A, Alia B, Mohamed B. Effect of Hardening Induced by Cold Expansion on Damage Fatigue Accumulation and Life Assessment of Aluminum Alloy 6082 T6. Mater Res 2012; 15(6): 981-985.

[28] Huang Y, Guan Z, Li H, Yang X, Li Z, Sun Y. Effects of chamfering, cold expansion, bolt clamping, and their combinations on fatigue life of aluminum-lithium alloy single plate. Adv Mech Eng 2018; 10(1): 1-13.

[29] Daniel H, Michael R, James C. Correlation of one-dimensional fatigue crack growth at cold-expanded holes using linear fracture mechanics and superposition. Eng Fract Mech 2011; 78: 1389-1406.

[30] Kumar SA, Bhattacharya A, Babu NCM. Fatigue crack growth life prediction around cold expanded hole using finite element method. International conference on advance manufacturing and materials engineering, 2014.

[31] Burlat M, Julien D, Levesque M, Bui-Quoc T, Bernard M. Effect of local cold working on the fatigue life of 7475-T7351 aluminum alloy hole specimens. Eng Fract Mech 2008; 75: 2042-2061.

[32] Huang Y, Guan Z, Li Z, Liu F. An Numerical Investigation on the Effect of the Combination of Cold Expansion and Interference Fitting on Fatigue Life Improvement of a 7075-T6 Aluminum Alloy Single Plate. 8th International Conference on Mechanical and Aerospace Engineering, 2017.

[33]Duprat D, Campassens D, Balzano M, Boudett R. Fatigue life prediction of interference fit fastener and cold worked holes. Int J Fatigue 1996; 18: 515-21.

[34] Yuan X, Yue Z, Wen S, Li L, Feng T. Numerical and experimental investigation of the cold expansion process with split sleeve in titanium alloy TC4. Int J Fatigue 2015; 77: 78-85.

[35] Farshbaf S, Chakherlou TN, Bakhshan H. Fatigue analysis of 7075-T6 aluminum alloy under high compressive residual stresses by considering the non-propagating crack region. Proc IMechE Part L: J Materials: Design and Applications 2022; 236(10): 1981-2001.

[36] Taghizadeh H, Chakherlou TN, Ghorbani H, Mohammadpour A. Prediction of fatigue life in cold expanded fastener holes subjected to bolt tightening in Al alloy 7075-T6 plate. Int J Mech Sci 2015; 90: 6-15.

[37] Wang X, Xu W, Zhang X, Zhang L, Hu B. Numerical prediction and experimental verification of fatigue life of TC4 plate strengthened by cold expansion. Journal of Zhejiang University, 2017; 50(8): 1610-1618.

[38] Xiao Z，Mao J，Hu D，Wang X，Wang R. Effects of Cold Expansion Process Parameters on Fatigue Life of GH4169 Superalloy. Journal of Propulsion Technology, 2022; 43(2): 210502.

[39] Ouyang X, Zhang X, Yang S. Finite Element Analysis and Fatigue Life Prediction of Cold Expansion. Journal of Propulsion Technology, 2011; 11(12): 2787-2791.

[40]Liu J, Wu H, Yang J, Yue Z. Effect of edge distance ratio on residual stresses induced by cold expansion and fatigue life of TC4 plates. Eng Fract Mech 2013; 109: 130-7.

[41]Luca S. The theory of critical distances: a review of its applications in fatigue. Eng Fract Mech 2008; 75: 1706-1724.

[42]Vallieres GM, Duquesnay DL. Fatigue life of cold-expanded fastener holes with interference-fit fasteners at short edge margins. Fatigue Fract Engng Mater Struct, 2015; 38: 574-582.

[43]Zhang X, Wang Z. Fatigue life improvement in fatigue-aged fastener holes using the cold expansion technique. Int J Fatigue 2003; 25: 1249-1257.

[44] Pasta S. Fatigue crack propagation from a cold-worked hole. Eng Fract Mech 2007; 74: 1525-1538.

[45] Mohan KS, Kumar VR. Fatigue crack prediction around non-cold worked hole. AIP Conference Proceedings 2019; 2148: 030035.

[46] Stefanescu D, Santisteban JR, Edwards L, Fitzpatrick ME. Residual Stress Measurement and Fatigue Crack Growth Prediction after Cold Expansion of Cracked Fastener Holes. J Aerosp Eng. 2004;17: 91-97.

[47] Taghizadeh H, Chakherlou1 TN, Aghdam AB. Prediction of fatigue life in cold expanded Al-

alloy 2024-T3 plates used in double shear lap joints. J Mech Sci Technol 2013; 27(5): 1415-1425.

[48] Lacarac VD, Garcia-Granada AA, Smith DJ, Pavier MJ. Prediction of the growth rate for fatigue cracks emanating from cold expanded holes. Int J Fatigue 2004; 26: 585-595.

[49] Newman JJC, Daniewicz SR. Predicting crack growth in specimens with overloads and cold-worked holes with residual stresses. Eng Fract Mech 2014; 127: 252-266.

[50] Wang Z, Zhang X. Predicting fatigue crack growth life for cold-worked holes based on existing closed-form residual stress models. Int J Fatigue 2003; 25: 1285-1291.

[51] Jones KW, Dunn ML. Predicting corner crack fatigue propagation from cold worked holes. Eng Fract Mech 2009; 76: 2074-2090.

[52] Chaboche J, Lesne P. A non-linear continuous fatigue damage model. Fatigue Fract Eng Mater Struct 1988; 11(1): 1-17.

[53] Bolotin VV. Mechanics of fatigue. Crc Press; 1999.

[54] Pinto AL, Talemi R, Araújo JA. Fretting fatigue total life assessment including wear and a varying critical distance. Int J Fatigue 2022; 156: 106589.

[55] Dowling, N. E. Mechanical behavior of materials: engineering methods for deformation, fracture, and fatigue. Prentice Hall international, 1993.

[56] Atzori B, Meneghetti G, Susmel L. Material fatigue properties for assessing mechanical components weakened by notches and defects. Fract Engng Mater Struct 2005; 28: 83-97.

[57] Lesuer DR, Kay GJ and LeBlanc MM. Modeling large strain, high-rate deformation in metals. In: Proceedings of the 3rd Biennial tri-laboratory engineering conference modeling and simulation, Pleasanton, CA, 3-5 November 1999; 3-5. Lawrence Livermor National Laboratory.

[58] Maximov JT, Duncheva GV and Amudjev IM. A novel method and tool which enhance the fatigue life of structural components with fastener holes. Eng Fail Anal 2013; 31: 132-143.

[59] Lim HJ, Lee YJ, Sohn H. Continuous fatigue crack length estimation for aluminum 6061-T6 plates with a notch. Mech Syst Signal Pr 2019; 120: 356-364.

[60] Champoux RL, Landy MA. Cold expansion of fastener and other holes using the split sleeve

system (Cx) and countersink cold expansion Nosecap (CsCx), FTI engineering process specification FTI 8101B. Fatigue Technology Inc 1984.